Electrochimica Acta 139 (2014) 21–28

Contents lists available at ScienceDirect

Electrochimica Acta

journal homepage: www.elsevier.com/locate/electacta

Core-shell TiO_2@C: towards alternative supports as replacement for high surface area carbon for PEMFC catalysts

Alessandro Zana[a,*], Celine Rüdiger[b], Julia Kunze-Liebhäuser[b], Gaetano Granozzi[c], Nini E.A. Reeler[a,e], Tom Vosch[a], Jacob J.K. Kirkensgaard[d], Matthias Arenz[a]

[a] Nano-Science Center, Department of Chemistry, University of Copenhagen, Universitetsparken 5, DK-2100 Copenhagen Ø, Denmark
[b] Physics Department E19, Technical University of Munich, James-Franck-Str. 1, D-85747 Garching, Germany
[c] Department of Chemical Sciences, Via Marzolo 1, 35131 Padova, Italy
[d] Niels Bohr Institute, University of Copenhagen, Universitetsparken 5, DK-2100 Copenhagen Ø, Denmark
[e] Sino-Danish Center for Education and Research (SDC) Niels Jensens Vej 2, Aarhus DK-8000, Denmark

ARTICLE INFO

Article history:
Received 22 May 2014
Received in revised form 27 June 2014
Accepted 3 July 2014
Available online 11 July 2014

Keywords:
proton conducting membrane electrolyte fuel cells
electrocatalysts
catalyst support materials

ABSTRACT

In this work, corrosion resistant TiO_2@C powder was tested as possible alternative to standard carbon black supports for polymer electrolyte membrane fuel cells. We separately prepared a stock solution of well-defined Pt nanoparticles and different support materials, and thereafter supported the NPs on the respective supports. As result we obtained high Pt dispersion on TiO_2@C supports comparable to conventional high surface area Pt/C catalysts. Accelerated stress tests were carried out in accordance with the Fuel Cell Commercialization Conference of Japan recommendations. The tests demonstrated improved corrosion resistance of Pt/TiO_2@C (as compared to Pt/C) when probing start/stop or mixed load cycle and start/stop conditions, whereas similar stability was observed when probing load cycle conditions only.

1. Introduction

Polymer electrolyte membrane fuel cells (PEMFCs) are becoming a feasible candidate for applications in portable and automotive industries. The development of carbon supported high surface area catalysts has resulted in a significant decrease of the amount of precious metals used. However, the stability and durability of these catalysts has to be improved [1,2]. As pointed out by Debe, improving the oxygen reduction reaction (ORR) activity may no longer be the most important goal for large scale automotive membrane electrode assembly (MEA) production [3]. Instead durability and power targets are the most important challenges. Thus the understanding of surface area and activity loss mechanisms becomes the key factor for the development of a stable and efficient support material. In state of the art catalysts carbon is used as a support material because of its high electrical conductivity and porous structure. However under MEA working conditions, such as dynamic load operation [4], and especially during start-up and shut-down, carbon is thermodynamically unstable [5–7]. Carbon corrosion might cause diverse and severe problems such as: Pt nanoparticle (NP) detachment, NP agglomeration and sintering as well as the structural collapse of the catalyst layer with consecutive loss of porosity of the catalyst layer [8]. These degradation mechanisms lead to a severely reduced lifetime of PEMFCs and inhibit the suitability of high surface area carbons (HSACs) for large scale automotive purposes.

Thus the development of alternative, more durable and corrosion resistant supports is needed. In order to develop a new support material some requirements should be considered. Ideally the new support should exhibit the following properties [9]: i) high electrically conductivity; ii) high porosity: iii) high stability under MEA working conditions; iv) the support material should have a reasonable BET surface area; v) the material costs must be contained. According to the requirements, metal oxides (MOs) with their reduced and doped phases are one of the possible alternatives to HSA carbon supports due to their high stability in a wide potential window, high tolerance to acid and oxidative environments and good mechanical stability [4,9]. Among MOs, Titania matches most of the requirements needed to be implemented as a possible support for HSA catalysts. For example, the surface area and structure of TiO_2 powders nicely match the support requirements for PEMFC applications. However TiO_2 is a wide band gap semiconductor ($E_g \sim 3$ eV) and its low electrical conductivity

* Corresponding author.
E-mail addresses: alessandro@chem.ku.dk (A. Zana), m.arenz@chem.ku.dk (M. Arenz).

http://dx.doi.org/10.1016/j.electacta.2014.07.002
0013-4686/

prevents its application in fuel cells. In the recent years many attempts have been reported to overcome the limited conductance of TiO_2 by using reduced phases of TiO_2, by doping TiO_2, or by modifying the surface oxide [9–12].

The aim of this study is to develop a Pt based catalyst with improved stability and comparable ORR activity to standard Pt/C catalysts in terms of mass (MA) and specific activity (SA). We describe the preparation and evaluation of a new catalyst support based on core-shell TiO_2@C powders. In order to evaluate the support properties, we prepared Pt/TiO_2@C, Pt/TiO_2, and Pt/C catalysts using Pt NPs from the same mother suspension prepared by a colloidal ethylene glycol route [13,14]. The physical properties of the resulting catalysts, i.e. the resulting Pt NP distributions were characterized by transmission electron microscopy (TEM) and small angle X-ray scattering (SAXS); the electrochemical and electrocatalytical properties by ex-situ investigations in electrochemical half-cells. The corrosion resistant properties of the catalysts have been tested by subjecting them to accelerated stress tests (ASTs) in accordance with the Fuel Cell Commercialization Conference of Japan (FCCJ) recommendations. These ASTs simulate the potential conditions experienced by the catalyst layer in an MEA under start-stop and load cycle conditions [7]. In addition we used a third AST treatment applied in our previous work, which combines simulation of load cycles and start-stop conditions.

2. Experimental

2.1. Catalyst Synthesis

TiO_2@C synthesis. - The core-shell TiO_2@C support was synthesized by a high temperature treatment of commercial anatase TiO_2 nanopowder (< 25 nm, 99.7% trace metal basis, specific surface area 45-55 $m^2\,g^{-1}$, Sigma-Aldrich, Germany) with acetylene (C_2H_2, solvent-free, Linde, Germany) in a horizontal quartz tube reactor (Carbolite, HST 12/600 with a Eurotherm 3216 controller, England) under continuous gas flow. For this purpose 0.35 g of the anatase TiO_2 powder were ground with mortar and pestle, distributed as a ~1 mm thick layer on a quartz plate and placed in the center of the oven. Before heating, the reactor was purged with argon (Ar 4.8, Linde, Germany) until it was air-free. During the heating procedure, the Ar gas flow was kept constant at 200 sccm (mass flow controller for 500 sccm N_2, calibrated for Ar, MKS Instruments, Germany). The powder was treated according to the following temperature-time protocol: 10 °C/min ramp from room temperature to 600 °C, plateau for 2 hours, 10 °C/min ramp to 800 °C and plateau for 2 hrs. Shortly after 600 °C were reached, 1 sccm of C_2H_2 (mass flow controller for 5 sccm C_2H_2, MKS Instruments, Germany) were added for 20 min to the Ar gas flow (flow fraction of ~0.5%). After annealing the reactor was allowed to cool under a constant Ar flow of 750 sccm. Due to the distribution of the powder batch as thin layer, the gradient in composition from top to bottom of the sample is assumed to be negligible. However a lateral variation in chemical composition along the gas flow and possible small variations from the target temperature could be inferred from color variations of the powder layer from dark grey at the edge of gas inlet to lighter grey towards the direction of gas outlet. For the preparation of the Pt/TiO_2@C catalyst, only the powder of homogeneous light grey color was used. As the results (see below) indicate no phase transition to rutile occurred under the used conditions.

Pt/X (X = C, TiO_2 and TiO_2@C) synthesis - The synthesis of the electrocatalysts consisted of two main steps. First, a stock suspension of colloidal Pt NPs with narrow size distribution was prepared via an ethylene glycol (EG) [6] route. Then the Pt NPs were precipitated from the EG-solution, resolved in acetone and deposited onto the different support materials. A detailed description of the Pt NP synthesis can be found in refs. [13,14]. Briefly, first an ethylene glycol solution of NaOH (50 mL, 0.4 M) is mixed with an ethylene glycol solution of $H_2PtCl_6{\cdot}H_2O$ (50 mL, 1.0 g) under vigorous stirring, in order to obtain a yellowish platinum hydroxide or oxide colloidal solution. The mixing is performed under an inert atmosphere of Ar. Then the colloidal solution is heated to 160 °C for 3 h obtaining a blackish-brown homogeneous metal particle colloidal suspension. The size and structure of the thus synthesized Pt NPs is controlled by transmission electron microscopy (TEM). The average diameter of the obtained Pt NPs is typically around 2 nm exhibiting a narrow size distribution. In order to support the Pt NPs onto the support materials, Ketjenblack- EC300 carbon support (AkzoNobel), TiO_2@C and the commercial anatase TiO_2, first 40 mL of HCl (1 M) is added to the colloidal NP solution for precipitation. The solution is centrifuged (4000 rpm, 6 min) and repeatedly washed in HCl before dispersing it in acetone. Then the Pt NPs are deposited onto the three support materials by mixing the NPs suspension with the support powder in 3 mL of acetone and sonicating for 1 h. Finally the catalyst is dried

2.2. Catalyst Characterization

Transmission electron microscopy - For the TEM investigations the catalyst dispersion was diluted by a factor of 1:10 and thereafter sonicated for 10 minutes. Afterwards 5 μL of the catalyst dispersion were pipetted onto a copper TEM grid (400 mesh; Plano, Germany) coated with a carbon film. To keep the catalyst loading low, after a few seconds the drop was adsorbed off the grid with a tissue. The grid was then dried and the catalyst investigated in a Tecnai T-20 G2 s-TEM (FEI) with an accelerating voltage of 200 kV. TEM imaging was performed before and after the AST treatments.

Small angle X-ray scattering - The platinum particle size distribution of the supported catalysts was determined by SAXS using a SAXSLab instrument (JJ-X-ray, Denmark) equipped with a Rigaku 100 XL+ micro focus sealed X-ray tube and a Dectris 2D 300 K Pilatus detector. For a more detailed description concerning the instrumentation, the SAXS measurement details and fitting parameters the reader may refer to ref. [13].

X-ray photoelectron spectroscopy (XPS) - The chemical surface composition of the as-prepared TiO_2@C powder was investigated with XPS. Photoemission data were acquired in a custom designed ultrahigh vacuum (UHV) system equipped with a VG MK II Escalab electron analyzer, working at a base pressure of 10^{-10} mbar. Core level photoemission spectra (O 1s, Ti 2p and C 1s regions) were taken at room temperature in normal emission using a non monochromatized Mg Kα X-ray source (1253.6 eV). Powder samples were suspended in ethanol and drop casted on conductive carbon tape. After drying in air, the samples were introduced in the UHV system, outgassed for 1 hr, and finally analyzed. The spectrometer energy calibration has been carried out by using a gold sample (Au 4f at 84 eV). High resolution spectra (0.1 eV steps, 0.5 s collection time, 10 sweeps, 20 eV pass energy) were taken. Quantitative analysis of the obtained XPS spectra was performed using CasaXPS data-analysis software [15].

Raman Measurements - Raman spectroscopy was performed by placing a drop of the sample on a cleaned glass cover slip on an Olympus IX71 microscope and the sample was left to dry before measuring. A 514 nm CW Argon Ion laser (CVI Melles Griot 35MAP431-200) was aligned into the microscope. Two narrow bandpass filter centered at 510 and 514 nm (Semrock FF02-510/20-25 and FF01-514/3-25) were used to spectrally clean the laser source. The laser light was reflected in the microscope on a 70/30 beamsplitter (XF122 from Omega Filters) towards a 100X 1.3 NA immersion oil objective (Olympus UplanFL N) that focused the laser on the sample and collected the Raman signal. The power of the laser focused into a diffraction limited spot at the sample was

120 μW (241 kW/cm^2). A 514 nm longpass filter (Semrock LP02-514RE-25) was used to block the 514 nm laser light in the detection path. The Raman spectrum was recorded by using a PI Acton SpectraPro SP-2356 polychromator (600 g mm-1 blazed at 500 nm) and a PI Acton SPEC- 10:100B/LN_eXcelon Spectroscopy System with a back-illuminated CCD chip (1340 × 100 pixels). Xaxis calibration of the spectra was performed after the measurements using a toluene Raman spectrum and a Neon pencil calibration lamp (ORIEL instruments, 6032 neon lamp). No further modifications or corrections were performed on the spectra.

Brunauer, Emmett and Teller (BET) isotherm measurements - We used the BET method by N_2 adsorption to determine the surface area of the TiO_2@C substrate [16].

2.3. Electrochemical Measurements

All the electrochemical measurements were performed in an all-Teflon three compartment electrochemical cell using a three electrode set up [17]. A rotating disk electrode (RDE; Radiometer analytical, France) with a glassy carbon (GC) tip was employed as working electrode (WE). The potential was controlled by a home-built potentiostat; the reference electrode was a saturated calomel electrode (SCE), located in a side compartment separated by an electrolytic bridge from the WE compartment in order to avoid chloride contaminations [18]. All potentials are given with respect to the reversible hydrogen potential (RHE), which was experimentally determined in RDE measurements. In the ORR measurements a platinum wire was used as counter electrode (CE), whereas the AST treatments were performed using a graphite rod as CE. The electrolyte was prepared using Millipore Milli-Q water (> 18.3 MΩ cm, TOC < 5 ppb) and concentrated $HClO_4$ (suprapure; Merck Germany).

The catalyst suspensions for the thin film RDE measurements were prepared by ultrasonically dispersing the respective catalyst powder for at least 15 minutes in ultrapure water. The amount of Pt per ml of water was 0.14 mg_{Pt} ml^{-1}. Before use the catalyst suspension was sonicated for 5 minutes and during the ultrasonic agitation 20 μl of the ink were withdrawn, pipetted onto the GC tip and left to dry at room temperature. The resulting Pt loading on the GC tip was 14 μg_{Pt} cm^{-2}. Thereafter the WE was transferred into the electrochemical cell and immersed in Ar saturated 0.1 M $HClO_4$ solution. Before starting the measurements the catalyst samples were cleaned by continuous potential cycling between 0.1 and 1.1 V_{RHE} until a stable and clean cyclic voltammogram of Pt was observed. For the RHE determination the electrolyte was saturated by hydrogen a polarization curve of the hydrogen evolution/hydrogen oxidation reaction recorded. The nominal electrochemical Pt surface area (ECSA) was determined in CO stripping measurements. I.e. carbon monoxide was adsorbed at the catalyst at a potential of 0.05 V_{RHE} and afterwards the CO was replaced from the electrolyte by purging with Ar for 10 minutes at the same electrode potential. Finally CO was electrochemically oxidized by cycling the potential between 0.05 and 1.2 V_{RHE} with a scan rate of 50 mVs^{-1}. The specific activity (SA) of the ORR was determined in O_2 saturated electrolyte from the positive going RDE polarization curve recorded at a scan rate of 50 mVs^{-1} and at a rotation speed of 1600 rpm. The polarization curves were corrected for the non-faradaic background currents by subtracting the cyclic voltammogram (CV) recorded in Ar saturated electrolyte.

2.4. Accelerated stress test protocols (AST)

The degradation resistance of the different catalysts was tested using three different degradation protocols based on fuel cell commercialization conference of Japan (FCCJ) recommendations [7]. Treatment I simulates load-cycle conditions in a MEA and consisted of applying square waves potentials, i.e. holding the WE for 3s at the lower (0.6 V_{RHE}) potential and 3s at the upper (1.0 V_{RHE}) potential for 9000 potential cycles. The second protocol, treatment II, consisted of potential cycles between 1 and 1.5 V_{RHE} with a sweep rate of 500 mVs^{-1} for a total of 12000 cycles. The aim of treatment II is to simulate conditions experienced by an MEA during start-up and shut-down. For a better understanding of treatment I and II the reader is referred to ref. [7]. The third protocol, treatment III, consisted of potential cycles between 0.4-1.4 V_{RHE} with a sweep rate of 500 mVs^{-1} for a total treatment of 3600 potential cycles. Treatment III was chosen to simulate combined load cycle and start-up/shut-down conditions and to compare the results with our previous investigations [19,20]. All measurements were conducted at room temperature and without rotation. ECSA measurements were performed at the beginning and at the end of each AST protocol.

Table 1a
at. % of components in O1s region.

C-O, O-C=O	H_2O, ester or carboxyl	OH (ads)	O-Ti (TiO_2)
0	2.2	17.0	80.8

Table 1b
at. % of components in Ti2p region.

TiO_2	Ti^{3+}	Ti^{2+}	TiC
92	0	2.8	5.2

Table 1c
at. % of components in C1s region.

O-C=O	C=O	C-O(H)	C-C	C-Ti
6.1	6.3	28	59	0.6

3. Results and discussion

The core shell TiO_2@C powder obtained from the heat treatment of TiO_2 in C_2H_2 has been characterized by several different techniques such as BET, XPS, Raman and HR-TEM. We start the discussion with the elucidation of the TiO_2@C composition using XPS. As expected Ti, C, and O were detected in the spectra. From a survey spectrum the relative (surface) composition of the powder was estimated to be Ti:O:C ~ 1:3:1. In Fig. 1 the measured XPS regions are displayed together with the different components obtained after a standard deconvolution procedure. The binding energy (BE) of the spectra was corrected relative to the expected position of the $Ti2p_{3/2}$ peak (TiO_2 component at BE = 258.6 eV) to correct for possible charging effects [21]. Table 1a-c summarizes the quantitative analysis of the individual regions (in at% of each component). The peaks in the Ti2p and O1s region indicate that most species are associated with TiO_2. With a total fraction of 8 at%, there is only a small amount of TiC and Ti^{2+} (most likely TiO) present on the surface. The TiC formation may be due to the diffusion of C into the TiO_2 during the heat treatment [22]. The detected oxygen is mainly bound in TiO_2 or present in form of adsorbed OH species (most likely from water). In the C1s region the contribution from graphitic carbon is responsible for more than half of the peak intensity, followed by carbon bound to different oxygen containing groups. In conclusion, XPS indicates that the support mainly consists of TiO_2, C, and small amounts of a TiC phase.

A standard method to investigate the nature of carbon materials is Raman spectroscopy. In Fig. 2 the Raman spectra of the TiO_2@C support (Fig. 2c) are compared to spectra of Ketjenblack EC300 (Fig. 2a), which is a standard high surface area carbon used

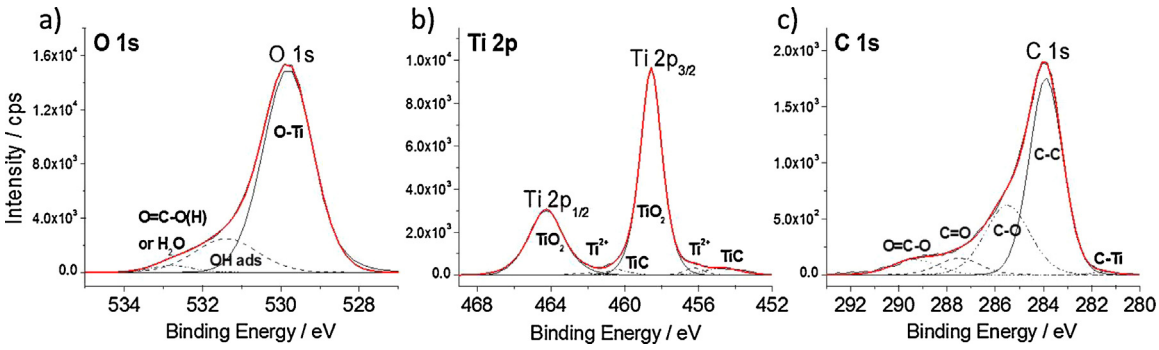

Fig. 1. High resolution XPS spectra of as prepared TiO_2@C powder with component fits. a) O1s region, b) Ti2p region, c) C1s region.

as support in fuel cell catalysts, and TiO_2 anastase (Fig. 2b), which was used as precursor for the TiO_2@C support. For TiO_2@C and Ketjenblack EC300 the main features in the spectra are associated to carbon, graphitic (G peak at about 1600 cm^{-1}) and defect (D1 peak at about 1340 cm^{-1}). The fact that both carbon features occur on TiO_2@C as on Ketjenblack EC300 indicates that the carbon shell on the TiO_2 particles has some similarities to the one detected for EC300. However, the intensity ratio between the D1 and G band in both samples is different. Studies on the degradation of high surface area carbons have shown that during an AST the D1 band decreases significantly due to the preferential consumption of defects [23,24]. The higher intensity of the G peak for the core-shell TiO_2@C particles therefore could indicate a more stable graphitized character of the carbon deposited during the heat treatment in C_2H_2 as compared to the high surface area carbon. In addition to the bands associated with carbon, in the spectra of TiO_2@C four peaks at c.a. 635 cm^{-1}, 516 cm^{-1}, 395 cm^{-1} and 145 cm^{-1} occur, which can be assigned to the different vibration modes of Anatase [25], see also comparison with Fig. 2b. From the Raman analysis, no different TiO_2 polymorphs were detected after heat treatment in C_2H_2. In agreement with the HR-TEM investigation (see below) the Raman spectra of the TiO_2@C show no formation of Graphene like structures.

The proposed core-shell structure of TiO_2@C is confirmed by electron microscopy. In Fig. 3 HR-TEM micrographs of the TiO_2@C support are shown. In Fig. 3a one can clearly identify the crystalline TiO_2 cores and the carbon layer wrapped around the TiO_2 NPs. In Fig. 3b a close-up of a single TiO_2@C support particle is seen. Here the highly crystalline core is even seen more clearly alongside the graphitic carbon shell, which has the typical structure of a carbon black with some graphitic character like VulcanXC72R or Ketjen black EC300.

A disadvantage of the heat treatment of TiO_2 in C_2H_2 is seen in the BET isotherms. The BET characterization indicates that the resulting TiO_2@C core shell powder exhibits a decreased surface

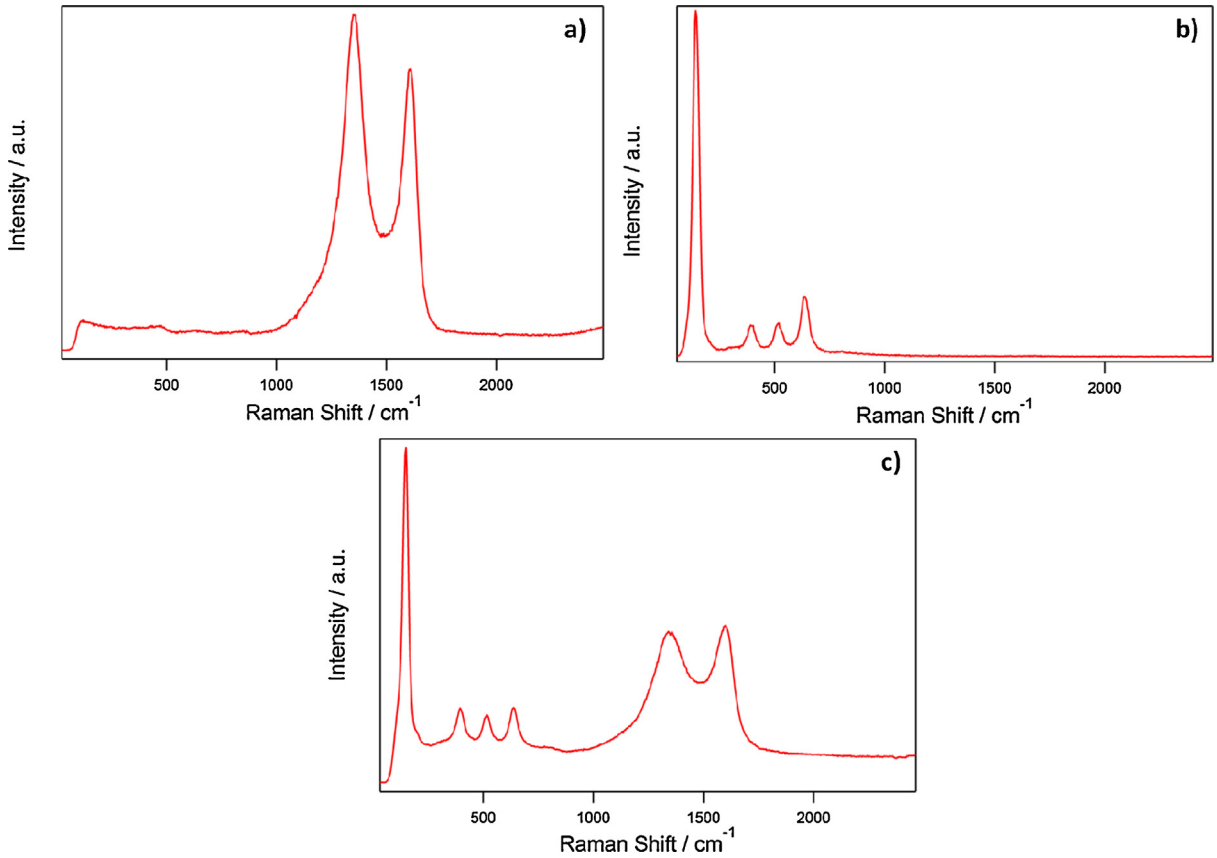

Fig. 2. Raman spectra of a standard Ketjenblack EC-300 carbon support (a), Anatase TiO_2 (b) and the synthesized TiO_2@C support (c).

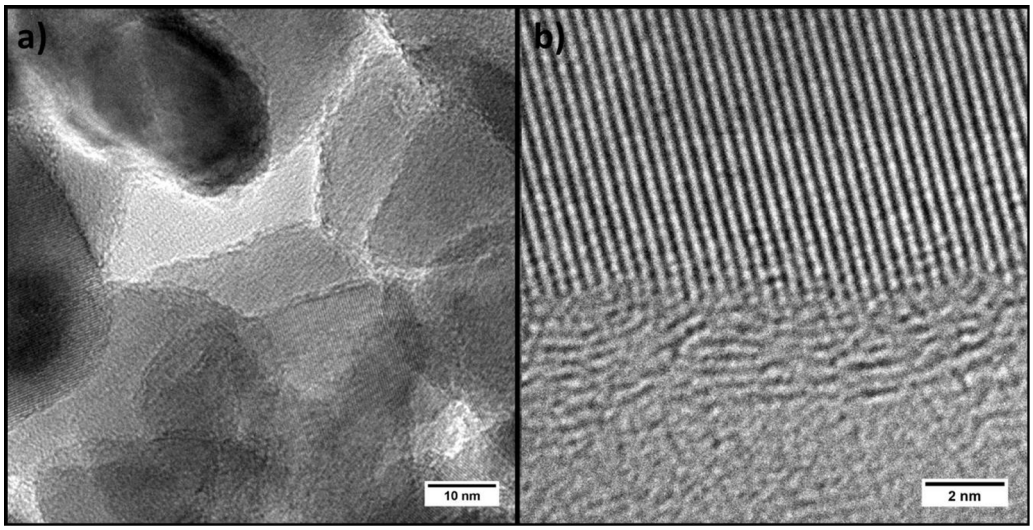

Fig. 3. HR-TEM of TiO_2@C a) and zoomed HR-TEM of TiO_2@C at the interface between TiO_2 and C b).

area of 14 $m^2 g^{-1}$ (see first row in Table 2) as compared to the starting anatase powder (BET area 50 $m^2 g^{-1}$). This decrease in surface area is undesired for fuel cell applications and is associated to a sintering process of the TiO_2 anatase powder during heat treatment. Nevertheless, as we show below at this point the heat treatment is necessary to obtain a conducting surface layer on the semiconducting anatase powder.

With the help of the different characterization techniques we have shown that we formed a core shell structure on the TiO_2 powder. In this process a minor amount of TiC phase is formed as indicated by XPS. The next step in our study was to deposit Pt NPs onto the TiO_2@C support. For comparison we also prepared respective catalysts on TiO_2 and Ketjenblack EC300 using the same Pt NP stock suspension. This enabled us to probe exclusively the influence of the support properties on the performance of the different catalysts in order to show the advantages and disadvantages of the TiO_2@C support. In total four samples were prepared, i.e. 10 wt.% Pt/TiO_2, 5 wt.% Pt/TiO_2@C, 10 wt.% Pt/TiO_2@C and 30 wt. % Pt/C.

The first electrochemical evaluation of catalysts is usually cyclic voltammetry (see figure S1 in the supporting information for the cyclic voltammograms of the 5 wt.% Pt/TiO_2@C and the 30 wt. % Pt/C sample). The pseudo capacitive currents observed in cyclic voltammetry are almost overlapping for the two supports (TiO_2@C and EC300), indicating that the semiconductive character of TiO_2 does not limit the electrical conductivity of the catalyst after a proper heat treatment process in acetylene. All features present in the CV of the Pt/TiO_2@C catalyst, such as H_{UPD} (0.1-0.3 V_{RHE}), the double layer region (0.3-0.5 V_{RHE}), and PtO_x formation and reduction (ca. 0.7 V_{RHE}) are almost identical to the one in the CV of the Pt/C sample. The respective nominal ECSA values of the catalysts, i.e. the ECSA calculated from the Pt amount used for synthesizing the catalyst, are listed in Table 2. The ECSA values for the 10 wt.% Pt/TiO_2, the 5 wt.% Pt/TiO_2@C and 10 wt.% Pt/TiO_2@C were 17 $m^2 g^{-1}$, 78 $m^2 g^{-1}$ and 61 $m^2 g^{-1}$, respectively. For the 30 wt. % Pt/C 80 $m^2 g^{-1}$ were obtained. i.e. whereas only very low nominal surface areas are obtained on the untreated TiO_2 supports, heat treatment of the TiO_2 powder enables values comparable to standard catalysts. Applying TEM the reason for these different nominal surface areas becomes apparent, see Fig. 4. While on Ketjenblack the Pt NPs are well distributed onto the support, on untreated TiO_2 only few Pt NPs are found on the support. Even though some minor agglomeration of the Pt NPs on the TiO_2 support is seen, the individual particle size obtained in TEM is still around 2 nm. Thus NP agglomeration cannot be the main factor responsible for the small nominal ECSA.

Instead, we propose that the low nominal ECSA of the 10 wt. % Pt/TiO_2 is due to two effects: i) the support only allows insufficient particle anchoring. This is indicated by the fact that in the TEM micrographs several Pt NPs are observed that are not attached to the support, but the carbon film of the TEM grid (Fig. 4b). Due to the insufficient anchoring a significant amount of Pt NPs is lost in the synthesis process; ii) since TiO_2 in bulk phase is a wide band gap semiconductor, another effect might be that the low conductivity of the support limits the rate of electron transfer processes from the Pt NP through the support to the GC electrode [11]. Most likely the largest contribution of the Pt signal in the ECSA measurements stems from unsupported NPs and only a minor part from the supported ones. This observation is in contrast to previous reports of Popov et al., who report that they attached Pt NPs to a TiO_2 substrate reaching ECSA values of ca. 31 $m^2 g^{-1}$. The discrepancy between their results and our findings might be due to the different strategy used to overcome the low electrical conductivity of TiO_2. By increasing the Pt wt.% loading up to 60 wt.% the authors claimed that Pt NPs not only acted as a catalyst but also provided a pathway for electrons [26,27].

Despite the fact that the BET area of the TiO_2@C support is lower than for the TiO_2 nanopowder depositing a carbon shell around the TiO_2 core, the ECSA can be significantly enhanced. In agreement with the ECSA measurements, the TEM micrographs in Fig. 4c, d

Table 2
BET area, ECSA, mean particle size determined by TEM and SAXS for the listed catalysts.

Catalyst	BET area of support ($m^2 g^{-1}$)	*ECSA ($m^2 g^{-1}$)	Pt particle size TEM (nm)	Pt particle size SAXS (nm)
30wt. % Pt/C	720	80	2.1	1.8
10wt. % Pt/TiO_2	50	17	2.1	-
10wt. % Pt/TiO_2@C	14	61	2.3	-
5wt. % Pt/TiO_2@C	14	78	2.3	2.2

*Nominal electrochemical active surface area (ECSA) assuming that all the Pt NPs are on the support

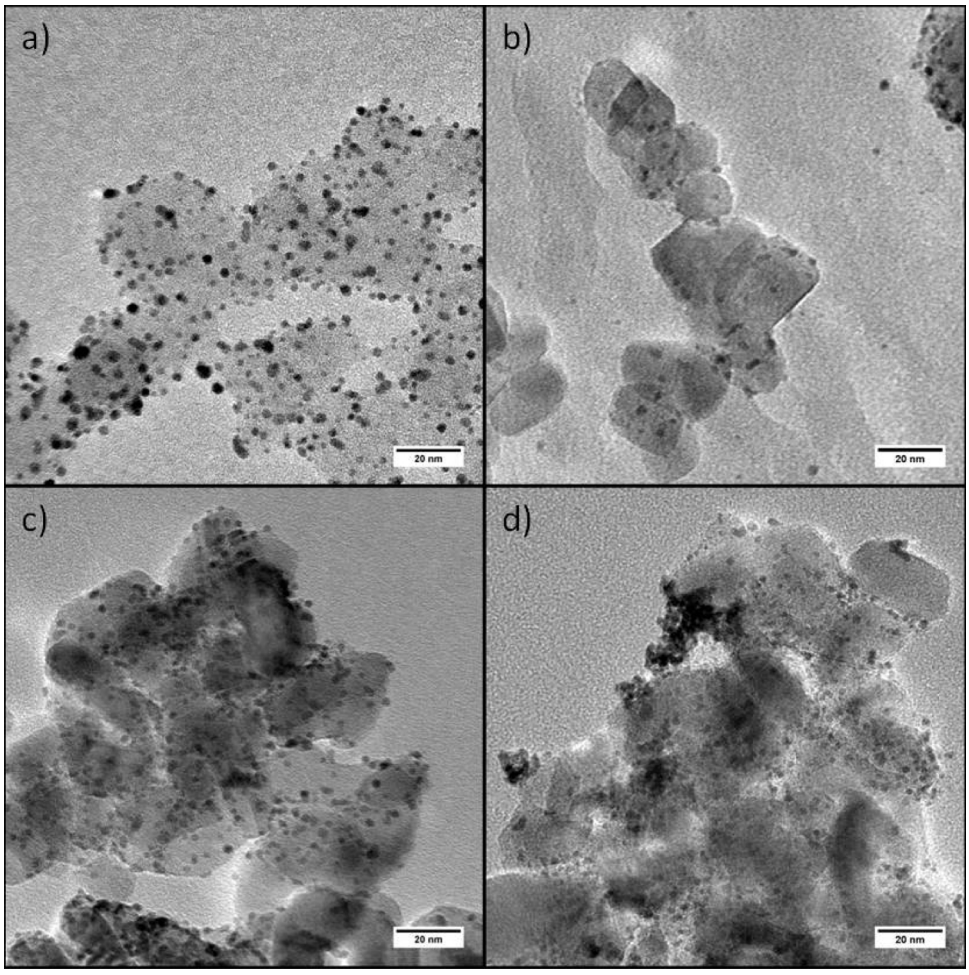

Fig. 4. TEM micrographs of 30wt%Pt/C (a), 10wt%Pt/TiO_2 (b), 5wt% Pt/TiO_2@C (c) and 10wt% Pt/TiO_2@C (d).

indicate that the optimal Pt loading on the TiO_2@C support is below 10 wt. %. While at 5 wt. % most Pt NPs are nicely distributed on the support and a high ECSA is obtained, at the 10 wt. % Pt/TiO_2@C sample NP agglomeration sets in. This is most likely due to the reduced surface area of the TiO_2@C support.

As mentioned above the TEM micrographs indicate that the average Pt NP diameter of the prepared catalysts is between 2.1 and 2.3 nm (see Table 2). Since TEM is a local technique, for the 30 wt.% Pt/C and 5 wt.% Pt/TiO_2@C samples the Pt size distribution of the macroscopic sample was also determined by SAXS. In Fig. 5 the respective size distribution curves are shown. As seen the narrow size distribution centered at 1.8 nm in case of the 30 wt. % Pt/C sample is only slightly shifted to higher values (2.2 nm) in case of 5 wt. % Pt/TiO_2@C sample, demonstrating that only very minor agglomeration occurs. The narrow Pt NPs distribution demonstrated by SAXS and TEM confirms, that the colloidal synthesis approach [13] is not only applicable for standard carbon supports, but also for the preparation using different support types if they are conducting. Especially for comparative studies as presented here, the colloidal method has the significant advantage over commonly applied impregnation techniques that no additional heat treatment in the catalyst synthesis is necessary. Such heat treatments change active phase (Pt NPs) and support at the same time making it difficult to relate seen changes to the support properties alone.

In the next step the catalytic performance of the prepared catalysts was probed. In Fig. 6 oxygen reduction reaction (ORR) measurements of the 5 wt.% and 10 wt.% Pt/TiO_2@C samples are compared with the 30 wt. % Pt/C catalyst. The ORR polarization curves of all catalysts are well defined and identical diffusion limited currents are reached. The parallel Tafel plots (inset) indicate that ORR on the 5 wt.% and 10 wt.% Pt/TiO_2@C samples follows the same reaction mechanism as on the 30 wt.% Pt/C sample. Furthermore, the measurements show that the lower surface area of the TiO_2@C support does not negatively influence the mass transport in RDE measurements. However, the ORR activity of the catalysts is slightly influenced by the support type, i.e. slightly higher overpotentials are seen on Pt/TiO_2@C support than for the Ketjenblack support.

The determined SAs and MAs (calculated at 0.9 V_{RHE}) are listed in Table 3. The SA and MA using the TiO_2@C supports are ca. 30% lower than the ones of the standard support, but the technological relevant MA is significantly higher (more than five times) than the one of the catalyst of the untreated TiO_2 powder. Thus we can conclude that even though the acetylene treatment significantly increases performance, further improvements are necessary to reach the activity performance of a carbon supported catalyst.

Table 3
SAs and MAs of the different catalyst samples calculated at 0.9 V_{RHE}. The MAs were calculated from the SA and the ECSA value given in Table 1.

Catalyst	$i_{s\,(0.9V)}$ ($mAcm^{-2}{}_{Pt}$)	$i_{m\,(0.9V)}$ ($Amg^{-1}{}_{Pt}$)
30 wt.% Pt/EC300	0.54	0.42
10 wt.% Pt/TiO_2	0.33	0.054
10 wt.% Pt/TiO_2@C	0.385	0.23
5 wt.% Pt/TiO_2@C	0.39	0.3

Table 4
Summary of the ECSA loss, determined by CO stripping, of the respective catalyst due to the AST treatments. Treatment I: 9000 potential steps between 0.6 and 1 V_{RHE} with a hold time of 3s; Treatment II: 12000 cyclic voltammograms between 1.0 and 1.5 V_{RHE} with a scan speed of 500 mVs^{-1}; Treatment III: 3600 cyclic voltammograms between 0.4 and 1.4 V_{RHE} with a scan speed of 500 mVs^{-1}.

Catalyst	AST treatment	Initial ECSA (m^2/g)	ECSA after AST (m^2/g)	ECSA area loss (%)
Pt/C	Treatment I	84.4	51.9	38.5
Pt/TiO_2@C	Treatment I	94	52.6	44
Pt/C	Treatment II	79.4	64.4	18.7
Pt/TiO_2@C	Treatment II	81.1	75	7.5
Pt/C	Treatment III	83.5	32.4	61.2
Pt/TiO_2@C	Treatment III	92.6	50	46

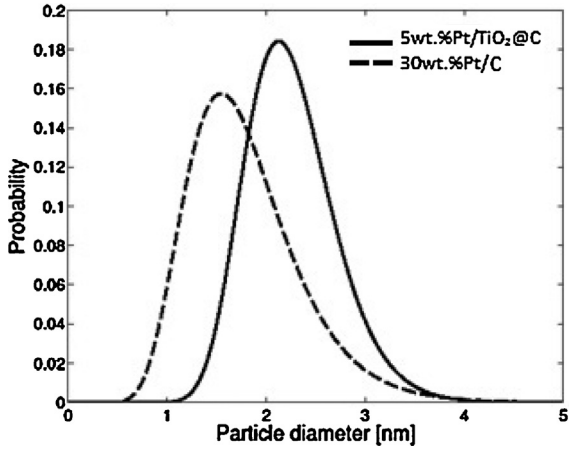

Fig. 5. SAXS particle size distribution curves for 5 wt. % Pt/TiO_2@C (black solid line) and 30 wt. % Pt/C (black dotted line). The average size distribution is centered at 1.8 ± 1.2 nm (FWHM taken as error) for 30 wt. % Pt/C, and at 2.2 ± 1.01 nm (FWHM taken as error) for 5 wt. % Pt/TiO2@C.

However, the main motivation of this study was not to probe the activity performance but to probe if oxide based supports limit or completely eliminate support corrosion. Due to the good compatibility in terms of ECSA, MA and SA between the 5 wt.% Pt/TiO_2@C and the 30 wt.% Pt/C samples we concentrated on these two catalysts for the AST treatments. The Pt/TiO_2 was not further investigated for stability as the MA performance was too poor.

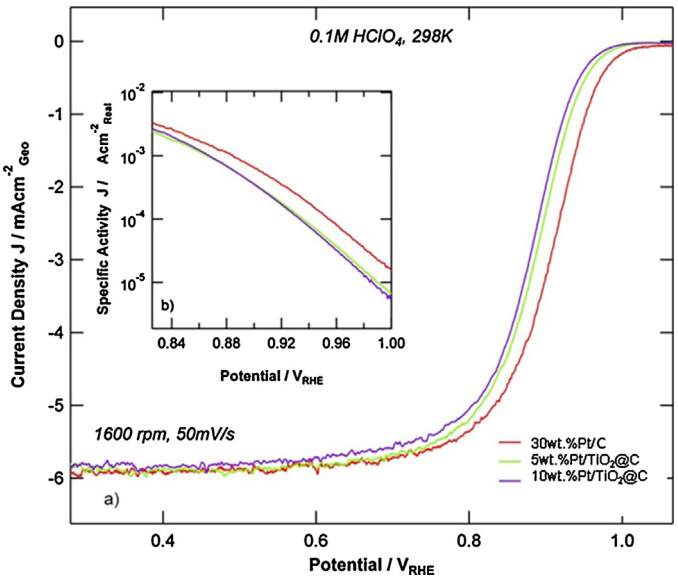

Fig. 6. (a) Oxygen reduction reaction (ORR) current densities for 30 wt.%Pt/C, 5 wt.%Pt/TiO_2@C and 10 wt.%Pt/TiO2@C. (b) Inset Tafel plot of the specific activities.

In Table 4 the differences in ECSA before and after each AST treatment are summarized. Treatment I consisted of potential steps between 0.6 - 1 V_{RHE} in order to simulate the conditions experienced by a fuel cell cathode under load cycle conditions [7]. At such conditions the ECSA loss of the two catalyst systems is almost identical in agreement with previous results indicating that under such conditions the ECSA loss of catalysts is mainly due to Pt dissolution [7,28,29] followed by Ostwald ripening and/or Pt migration and coalescence [30]. Under such degradation mechanisms, the role of the TiO_2@C support is limited, especially it is not expected that the support influences Pt dissolution. The situation changes when applying treatment II, which simulates start/stop conditions in fuel cells. In treatment II potential cycles between 1and 1.5 V_{RHE} are applied. This degradation conditions simulates the potential experienced at the cathode during start-up and shut-down. Under such condition, it is reported that the degradation of HSA Pt/C catalysts is mainly determined by carbon corrosion [6,7]. It is as also expected to be the main factor limiting the lifetime of fuel cells under real operating conditions with starting and shutting down of the fuel cell. The results show that the real advantage of the TiO_2@C support over conventional HSA carbons is reached under such conditions. Whereas the 5 wt.%Pt/TiO_2@C support loses only 7.5% of its surface area, under the same treatment the 30 wt.% Pt/C catalyst loses about two and a half times as much surface area (19%, Table 4). The improved stability of the TiO_2@C support under such demanding conditions is also seen in the comparison of the cyclic voltammograms recorded before and after the AST treatment (see supporting information): the capacity of the Pt/C catalyst is significantly increased after the treatment and a quinone/hydroquinone redox couple appears in the voltammogram, both indications for carbon corrosion. By comparison the cyclic voltammogram of the Pt/TiO_2@C catalyst almost remains unchanged. Only the peak associated with the reduction of OH species is slightly shifted to lower potentials. Last but not least the improved stability of the TiO_2@C is also seen in AST treatment III. Under such conditions the surface area loss of the Pt/TiO_2@C is reduced by roughly 30% as compared to the Pt/C catalyst (see Table 4).

4. Conclusions

The core shell TiO_2@C powder obtained from the heat treatment of TiO_2 in C_2H_2 has been tested as potential support for fuel cell catalysts. In order to compare the new support with reference samples we prepared Pt/C, Pt/TiO_2 and Pt/TiO_2@C catalysts using the same colloidal stock solution and avoiding any heat treatment steps, which might change the nanoparticle-substrate system. We demonstrate that indeed TiO_2@C exhibits interesting potential as alternative support for carbon. While the Pt NPs cannot be easily supported on untreated TiO_2 nanopowder, thanks to the conducting carbon shell the supporting step on TiO_2@C is as facile as for standard high surface area carbon supports. As a consequence Pt/TiO_2 fails to reach high ECSA values, but Pt/TiO_2@C exhibits the same nominal ECSA as Pt/C. Concerning stability, Pt/TiO_2@C exhibits significant improvements over Pt/C during the critical

start-stop conditions, while under load cycles approximately the same stability is seen. This observation is in agreement with the proposition that the catalyst stability under load cycles mainly depends on the properties of the active phase, i.e. the Pt NPs, while under start-stop cycles the support properties determine the stability. One might conclude that it is the latter conditions that offer the main potentials for improvements. At the same time one must take into account that the tests were performed at room temperature. At higher temperatures, in particular at 160°C, the operation temperature of HT-PEMFCs, the support should play a larger role for the catalyst stability.

Last but not least, one should note that the discussed TiO_2@C support needs further improvements. The BET area of the support is too low. Even though comparing carbon and oxide based supports one needs to account for the different molar weight when comparing BET areas, the reduction in BET due to the heat treatment in acetylene is unfavorable and needs improvements. Furthermore, the catalyst activity of Pt/TiO_2@C is reduced as compared to Pt/C. The reason for this is still unclear. This might be due to a negative particle proximity effect or a support particle interaction. These issues will be addressed in ongoing work.

Acknowledgments

The research leading to these results has received funding from the European Union Seventh Framework Programme (*FP7/2007-2013*) under *grant agreement* n° [*309741*] and from the Danish DFF through grant no. 10-081337. We acknowledge Keld West and Kell Mortensen from the University of Copenhagen for the BET measurements and discussions, respectively.

References

[1] R.T. Atanasoski, L.L. Atanasoska, D.A. Cullen, G.M. Haugen, K.L. More, G.D. Vernstrom, Electrocatalysis 3 (2012) 284–297.
[2] F. Ettingshausen, J. Kleemann, A. Marcu, G. Toth, H. Fuess, C. Roth, Fuel Cells 11 (2011) 238–245.
[3] M.K. Debe, Nature 486 (2012) 43–51.
[4] Y.J. Wang, D.P. Wilkinson, J.J. Zhang, Chem. Rev. 111 (2011) 7625–7651.
[5] J.P. Meyers, R.M. Darling, J. Electrochem. Soc. 153 (2006) A1432–A1442.
[6] C.A. Reiser, L. Bregoli, T.W. Patterson, J.S. Yi, J.D.L. Yang, M.L. Perry, T.D. Jarvi, Electrochem. Solid State Lett. 8 (2005) A273–A276.
[7] A. Ohma, K. Shinohara, A. Iiyama, T. Yoshida, A. Daimaru, ECS Transactions 41 (2011) 775–784.
[8] K. Sasaki, M. Shao, R. Adzic, Dissolution and stabilization of Platinum in Oxygen Cathodes, in: F.N. Buechi, M. Inaba, T.J. Schmidt (Eds.), in: Polymer Electrolyte Fuel Cell Durability, Springer, 2009.
[9] A. Rabis, P. Rodriguez, T.J. Schmidt, ACS Catal. 2 (2012) 864–890.
[10] L. Timperman, Y.J. Feng, W. Vogel, N. Alonso-Vante, Electrochimica Acta 55 (2010) 7558–7563.
[11] R. Hahn, F. Schmidt-Stein, J. Salonen, S. Thiemann, Y.Y. Song, J. Kunze, V.P. Lehto, P. Schmuki, Angew. Chem. -Int. Edit. 48 (2009) 7236–7239.
[12] T. Ioroi, Z. Siroma, N. Fujiwara, S. Yamazaki, K. Yasuda, Electrochem. Commun. 7 (2005) 183–188.
[13] J. Speder, L. Altmann, M. Roefzaad, M. Baumer, J.J.K. Kirkensgaard, K. Mortensen, M. Arenz, Physical Chemistry Chemical Physics 15 (2013) 3602–3608.
[14] Y. Wang, J.W. Ren, K. Deng, L.L. Gui, Y.Q. Tang, Chemistry of Materials 12 (2000) 1622–1627.
[15] N. Fairley, CasaXPS version 2.3.14dev38: Software package for VAMAS data processing, http://www.casaxps.com
[16] S. Brunauer, P.H. Emmett, E. Teller, Adsorption of gases in multimolecular layers, in: Journal of the American Chemical Society, 1938, pp. 309-319.
[17] K.J.J. Mayrhofer, G.K.H. Wiberg, M. Arenz, J. Electrochem. Soc. 155 (2008) P1–P5.
[18] K.J.J. Mayrhofer, S.J. Ashton, J. Kreuzer, M. Arenz, Int. J. Electrochem. Sci. 4 (2009) 1–8.
[19] J.C. Meier, C. Galeano, I. Katsounaros, A.A. Topalov, A. Kostka, F. Schuth, K.J.J. Mayrhofer, ACS Catal. 2 (2012) 832–843.
[20] K. Schlogl, M. Hanzlik, M. Arenz, J. Electrochem. Soc. 159 (2012) B677–B682.
[21] A.R. González-Elipe, G. Munuera, J.P. Espinos, J.M. Sanz, Surface Science 220 (1989) 368–380.
[22] Y. Zhang, T. Ichihashi, E. Landree, F. Nihey, S. Iijima, Science 285 (1999) 1719–1722.
[23] A. Zana, J. Speder, N.E.A. Reeler, T. Vosch, M. Arenz, Electrochimica Acta 114 (2013) 455–461.
[24] M. Hara, M. Lee, C.-H. Liu, B.-H. Chen, Y. Yamashita, M. Uchida, H. Uchida, M. Watanabe, Electrochimica Acta 70 (2012) 171–181.
[25] D.A.H. Hanaor, C.C. Sorrell, Journal of Materials Science 46 (2011) 855–874.
[26] S.Y. Huang, P. Ganesan, B.N. Popov, Appl. Catal. B-Environ. 102 (2011) 71–77.
[27] S.-Y. Huang, P. Ganesan, B.N. Popov, ACS Catal. 2 (2012) 825–831.
[28] R.M. Darling, J.P. Meyers, J. Electrochem. Soc. 150 (2003) A1523–A1527.
[29] R.M. Darling, J.P. Meyers, J. Electrochem. Soc. 152 (2005) A242–A247.
[30] A. Zana, J. Speder, M. Roefzaad, L. Altmann, M. Bäumer, M. Arenz, J. Electrochem. Soc. 160 (2013) F608–F615.